CHAPTER IV

EXPERIMENTAL RESULTS AND DISCUSSION

4.1 Hot ductility of steel grade AISI L3

The dependence of the reduction of area and the maximum load on the test temperature are shown in Fig.4-1 for the specimens solidified and strained at various rates. The summary of characteristic temperatures (ZST ZDT and ΔT) at various test conditions is shown in Table 4-1.

For the slow cooling rate of 0.5°C/s the RA-curves for tensile test at slow strain rate of 2×10^{-3}/s shows a distinctive maximum value at 1160°C with reduction of area value nearly 100%. The reduction of area for this test condition remain above 90% in the temperature range between 1160°C and 900°C. The ZST and ZDT for this test condition is 1389°C and 1263°C, respectively. The ZST and ZDT of the test at the same slow cooling rate and high strain rate of 2×10^{-2}/s was detected at 1335°C and 1158°C,

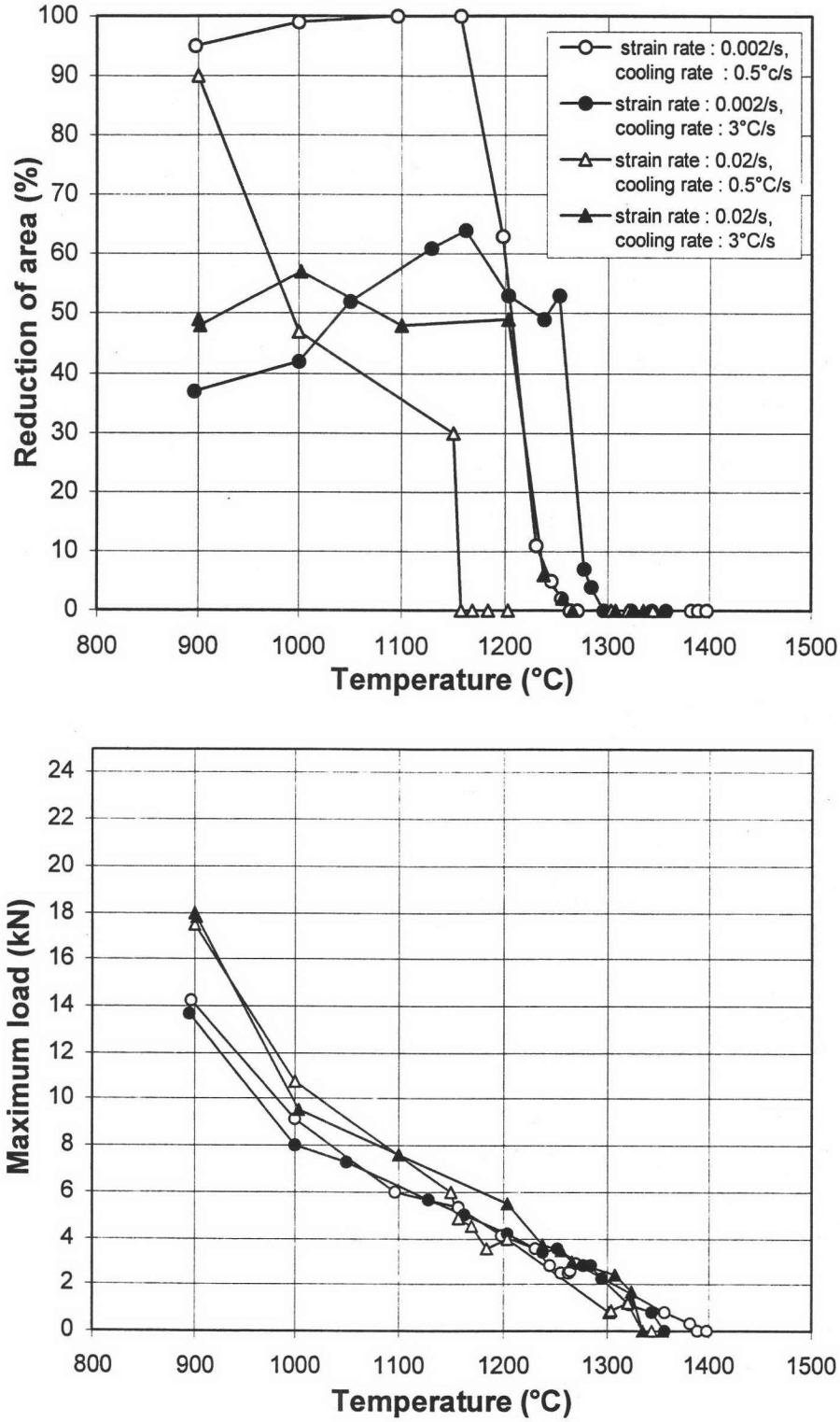

Fig.4-1 Reduction of area and the maximum tensile load versus temperature of the steel grade AISI L3.

Table 4-1 Characteristic temperatures of the steel grade AISI L3 at various test conditions.

Steel Grade	Test condition		ZDT	ZST	ΔT
	cooling rate (°C/s)	strain rate (/s)	(°C)	(°C)	(°C)
AISI L3	0.5	$2x10^{-3}$	1263	1389	126
	0.5	$2x10^{-2}$	1158	1335	177
	3	$2x10^{-3}$	1296	1357	61
	3	$2x10^{-2}$	1266	1335	69

respectively. The reduction of area for this test condition increased rapidly with the decreasing test temperature and the reduction of area is 90% at 900°C. It can be documented that the ZDT for tensile test at slow cooling rate from melting is shifted toward higher temperature with the decrease of strain rate from $2x10^{-2}$/s to $2x10^{-3}$/s. It is interesting to be noticed that the critical temperature range ΔT (the range of temperature between ZST and ZDT) is widened with the increasing strain rate (see Table 4-1).

At the fast cooling rate of 3°C/s and slow strain rate of $2x10^{-3}$/s the ZST and ZDT was detected at 1357°C and 1296°C, respectively. The RA-curve for this test condition shows the maximum reduction of area of 64% at

1162°C. This curve, then, gradually decline to lower reduction of area of 37% at 900°C. Tensile test at high strain rate of 2×10^{-2}/s shows the ZST and ZDT at 1335°C and 1286°C, respectively. The RA-curve show the maximum reduction of area of 56% at 1100°C and the reduction of area of 50-60% still occurring between the temperature range between 1200°C and 900°C. It can be noted that the ZDT in case of fast cooling rate from melting is shifted toward higher temperature with the decreasing strain rate. The critical temperature range ΔT is widened with the increasing strain rate (see Table 4-1).

Results from Table 4-1 indicated that the cooling rate significantly affected the ZST and ZDT. It can be noted that the fast cooling rate from melting resulted in shifting the ZDT toward higher temperature. The critical temperature range of fast cooling rate is smaller than that of slow cooling rate. The summary of the effect of cooling rate on critical temperature ΔT at different strain rate as mentioned above is shown in Fig.4-2.

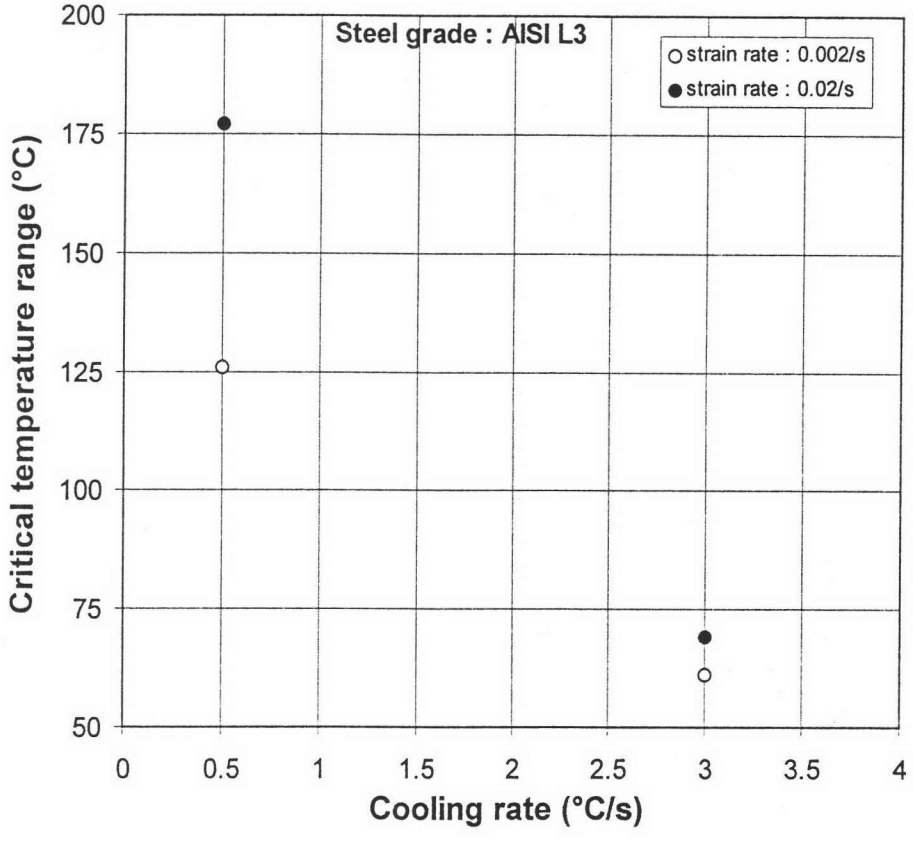

Fig.4-2 Characteristic temperature range between ZDT and ZST of steel grade AISI L3.

4.2 Metallographical investigation of steel grade AISI L3

The metallographical investigation is covering on the fractured specimen in tensile test and quenched specimen. The quenched specimen were analyzed to clarify the actual microstructure occurred during hot tensile test. The microstructure of fractured specimen is not the actual microstructure at hot tensile test temperature.

Because the specimen was cooled to room temperature, so the microstructure may be changed. Therefore the quenching test were carried out to investigate the microstructure. Due to the specimen of quenching test give rise to the microstructure that close to the actual microstructure at certain test temperature rather than that of the specimen of hot tensile test.

The microstructure of the specimen that cooled from melting at cooling rate of 3°C/s and then quenched from 1296°C is shown in Fig.4-3. This temperature is correspond to the ZDT for the hot tensile tests at the same cooling rate before tensile test at strain rate of 2×10^{-2}/s. Fig.4-3 shows the eutectic structure along interdendritic interface. Fig.4-4 shows the microstructure of a specimen quenched from 1266°C. This temperature is correspond to ZDT of the specimen in hot tensile test that was cooled from melting at cooling rate of 3°C/s before tensile test at strain rate of 2×10^{-3}/s. The Fig.4-4 shows that precipitates appear at the interdendritic boundaries, subsequently become the austenite grain boundaries. The white area is liquid phase and remains along grain boundaries at the time quenched. Fig.4-5 represents the microstructure of a specimen quenched from 1263°C. This is the ZDT for

cooling rate of 0.5°C/s before tensile test at strain rate of 2×10^{-3}/s. The microstructure shown in Fig.4-6 represents microstructure of a specimen quenched from 1158°C. This temperature is the ZDT for tensile test at cooling rate of 0.5°C/s before tensile test at strain rate of 2×10^{-3}/s. Both Fig.4-5 and Fig.4-6 show the precipitates located at the interdendritic boundaries as well as that in Fig.4-4. The Fig.4-4 to Fig.4-6 also displays remaining of liquid phase along the boundaries at the time quenched. The precipitates in the specimen shown in Fig.4-4 to Fig.4-6 were identified with using SEM-EDX. The microstructure shown in Fig.4-4 is micrograph taken with SEM and showed in Fig.4-7. The precipitates were identified with SEM-EDX as S, Mn, Fe and Cr, as shown spectrum in Fig.4-8, which is believed to be MnS or (Fe,Mn)S. Fig.4-9 shows the identified spectrum of the matrix as iron and chromium. Fig.4-10 shows the microstructure of the specimen cooled from melting at cooling rate of 3°C/s and quenched from 896°C. Fig.4-11 shows the microstructure of the same specimen as shown in Fig.4-10 but this photograph is taken with SEM. The microstructure in this sample represents the reduction of area of 37% in hot tensile test. The identified spectrum of the precipitate in Fig.4-12 showed S, Mn, Fe and Cr which could be MnS or (Fe,Mn)S.

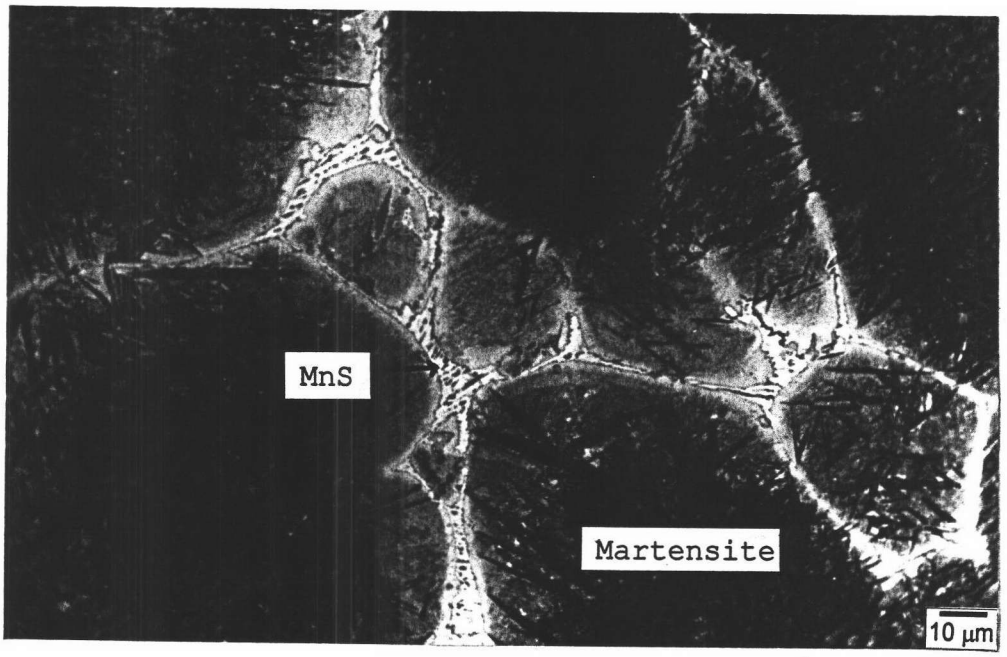

Fig.4-3 Sulfides precipitates along interdendritic region of specimen that solidified from melting with cooling rate of 3°C/s to 1296°C and then quenched.

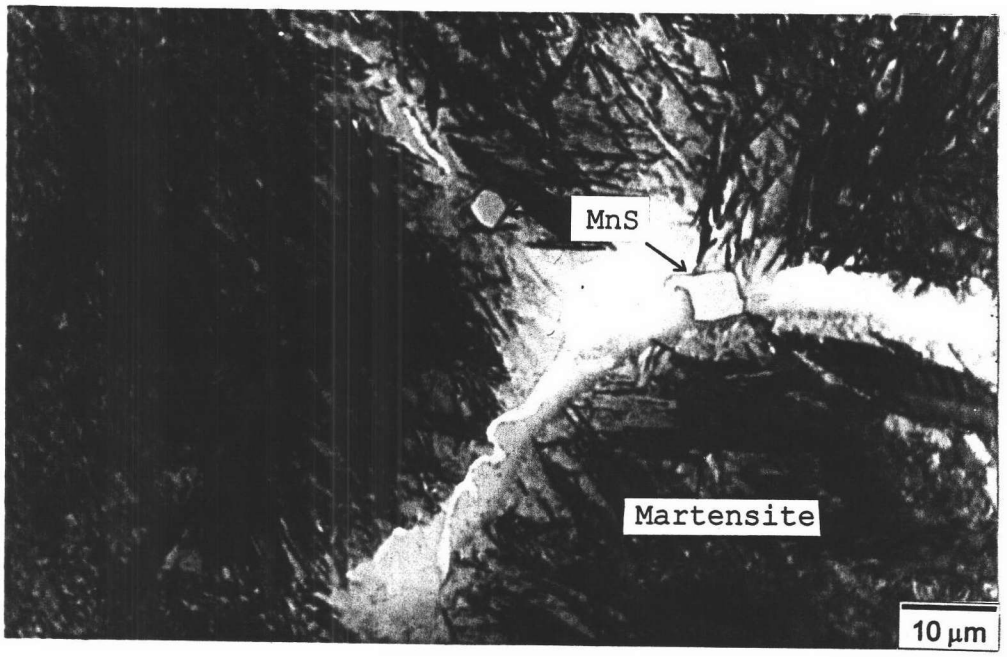

Fig.4-4 Sulfides precipitates along austenite grain boundaries of specimen that solidified from melting with cooling rate of 3°C/s to 1266°C and then quenched.

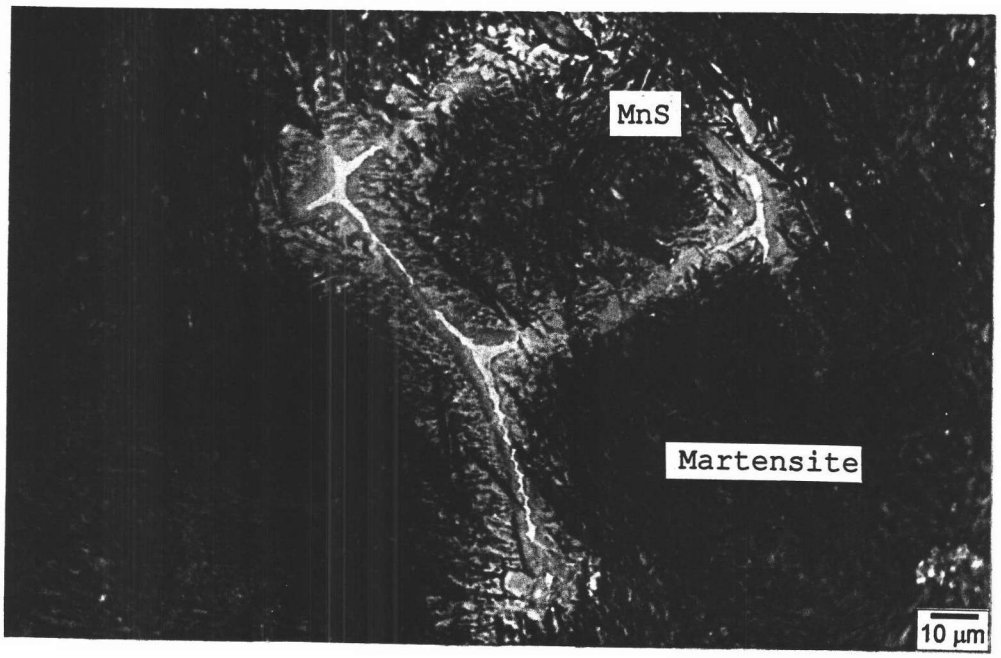

Fig.4-5 Sulfides precipitates along austenite grain boundaries of specimen that solidified from melting with cooling rate of 0.5°C/s to 1263°C and then quenched.

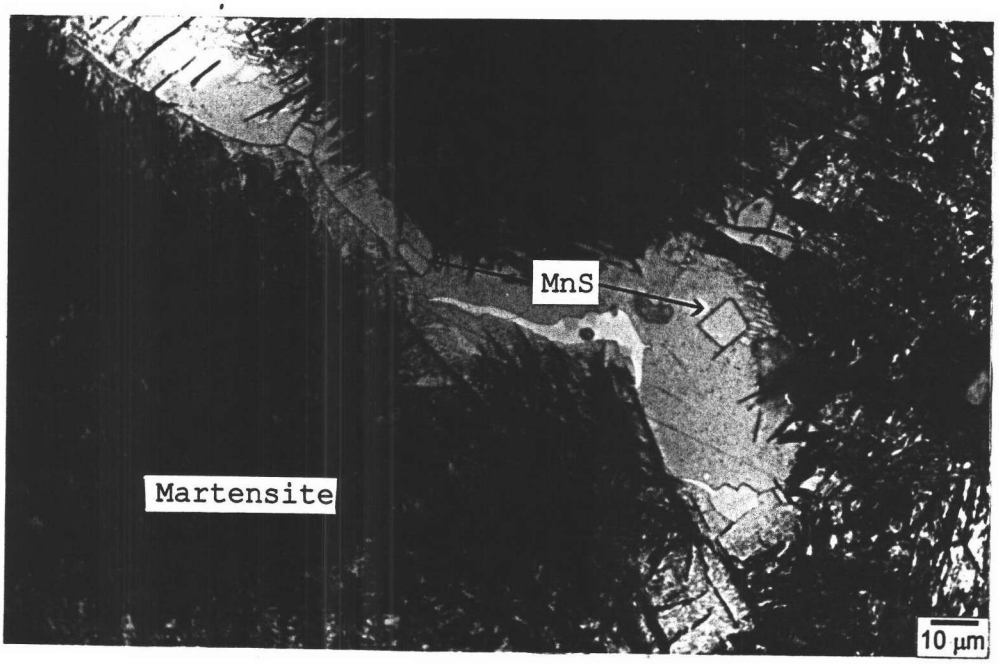

Fig.4-6 Sulfides precipitates along austenite grain boundaries of specimen that solidified from melting with cooling rate of 0.5°C/s to 1158°C and then quenched.

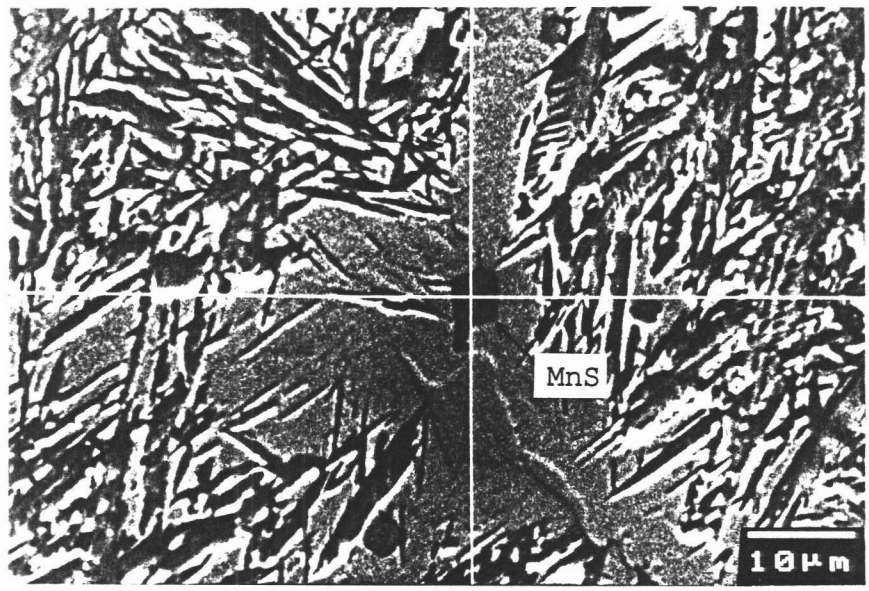

Fig.4-7 SEM-micrograph of sulfides precipitates of specimen that solidified from melting with cooling rate of 0.5°C/s to 1263°C and then quenched.

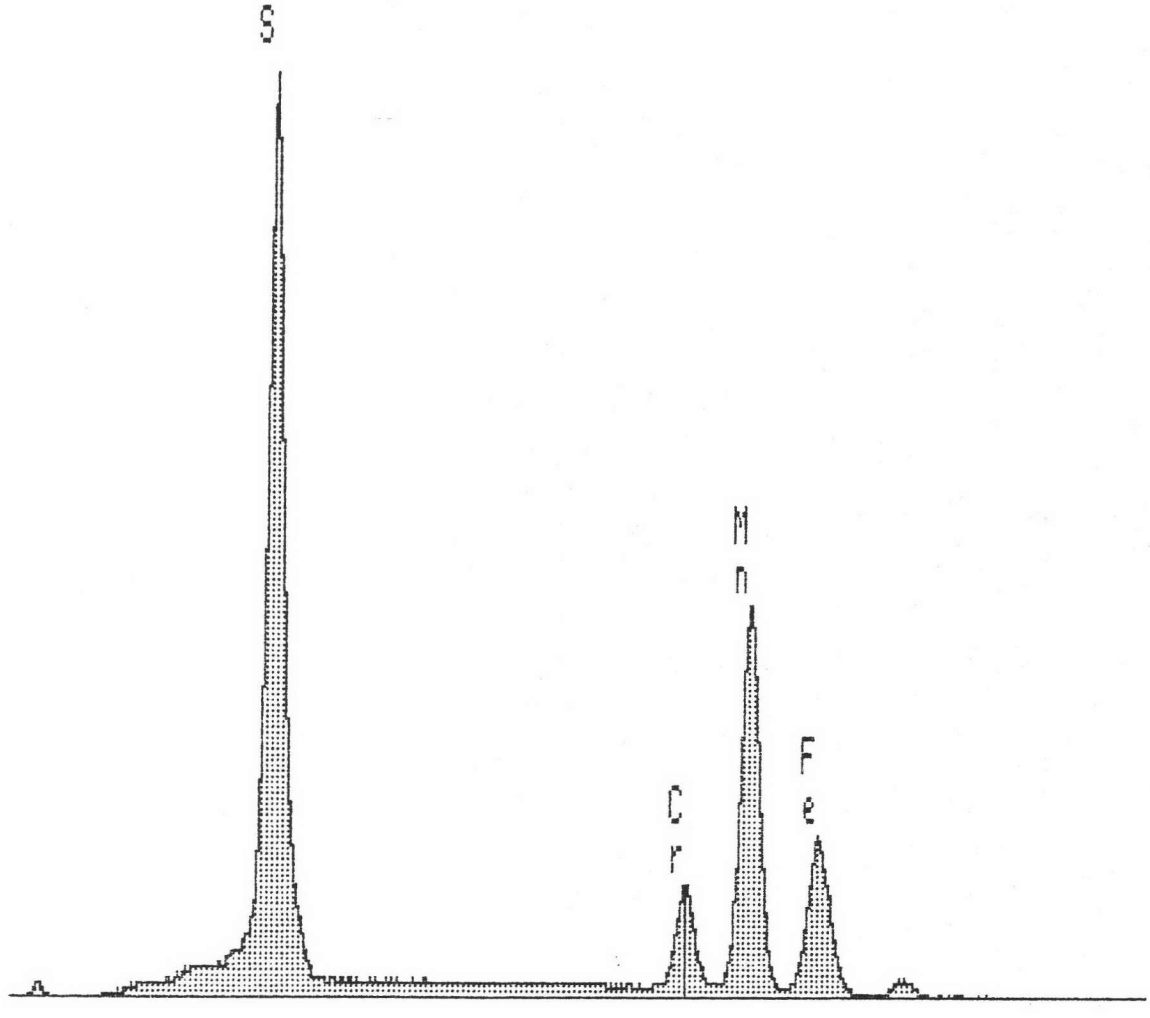

Fig.4-8 SEM-EDS analysis of sulfides precipitates of Mn and Fe of specimen that solidified with cooling rate of 0.5°C/s to 1263°C and then quenched.

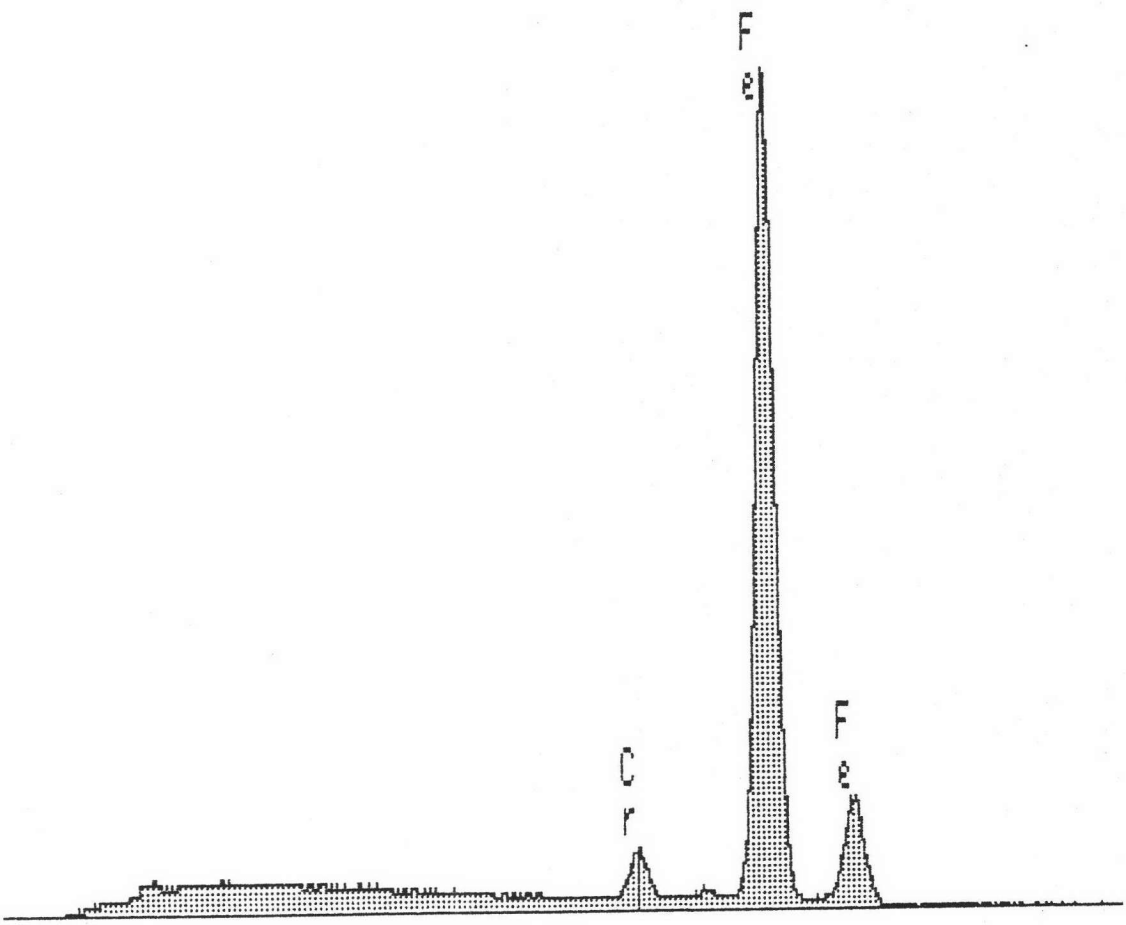

Fig.4-9 SEM-EDS analysis of iron-chromium matrix of specimen that solidified from melting with cooling rate of 0.5°C/s to 1263°C and then quenched.

Fig.4-10 Sulfides precipitates of specimen that solidified with cooling rate of 3°C/s to 896°C and then quenched.

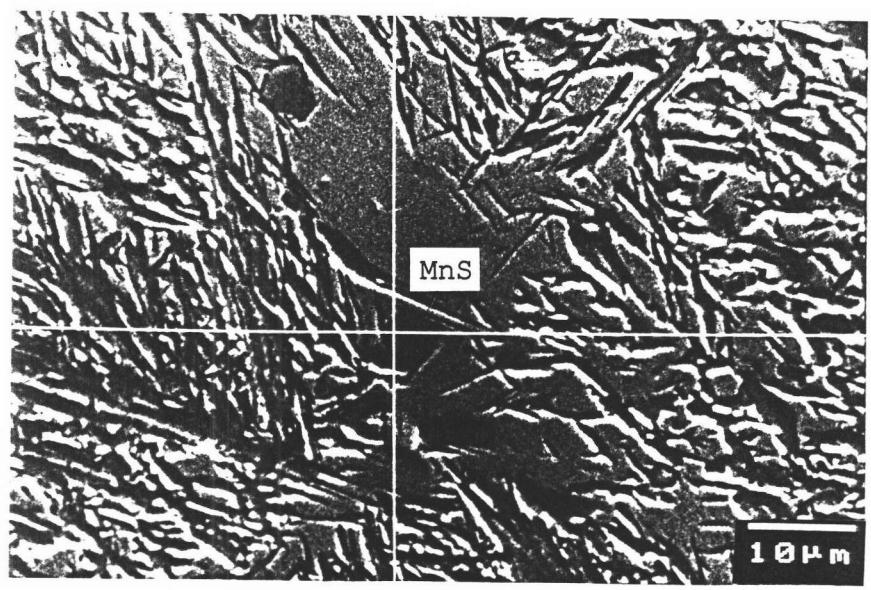

Fig.4-11 SEM-micrograph of sulfides precipitates of specimen that solidified from melting with cooling rate of 3°C/s to 896°C and then quenched.

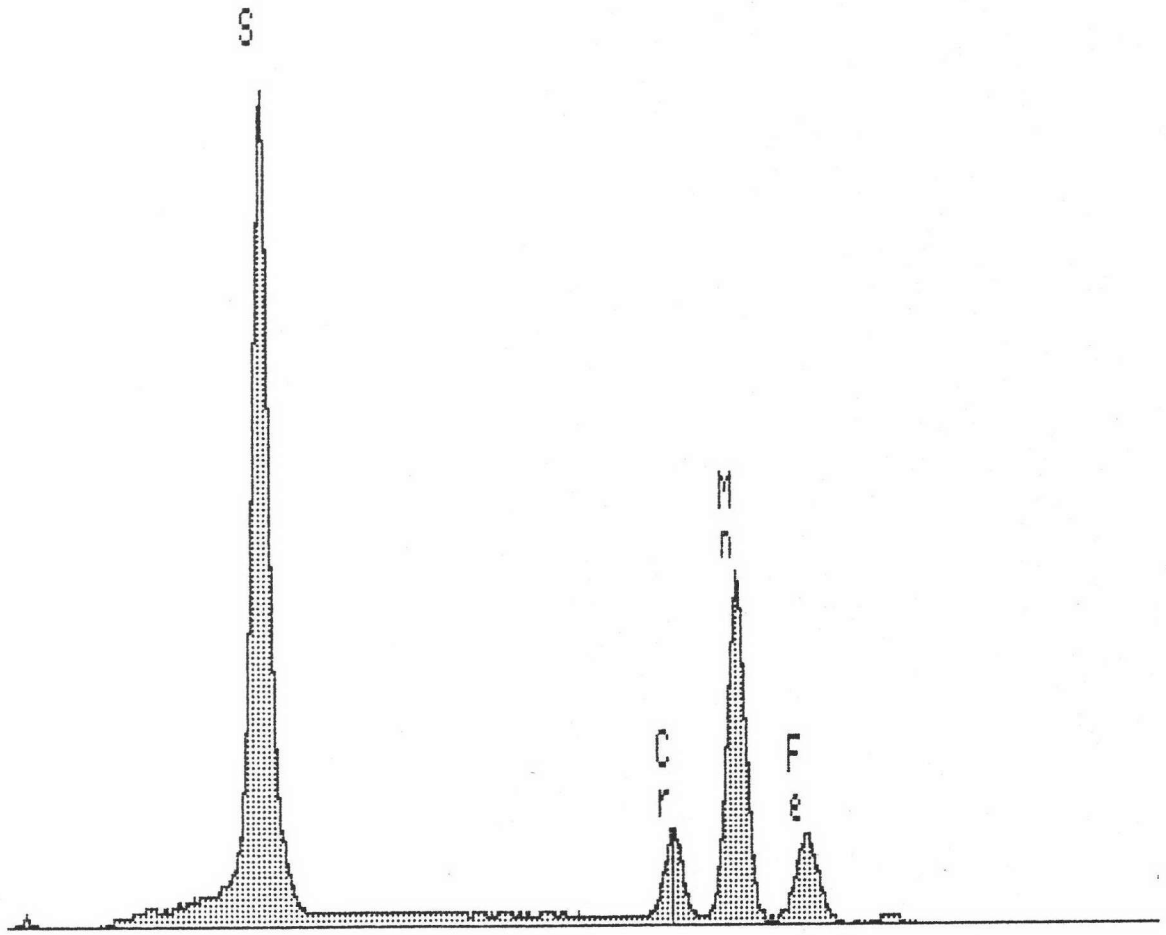

Fig.4-12 SEM-EDS analysis of sulfides precipitates of Mn, Cr and Fe of specimen that solidified from melting with cooling rate of 3°C/s to 896°C and then quenched.

4.3 Effect of cooling rate and strain rate on hot ductility of steel grade AISI L3

The results of hot tensile test shown in Fig.4-1 and Table 4-1 is significantly depend on the test variables. The tensile test at various strain rates after cooled at various cooling rates from melting affected the widening of critical temperature range.

The critical temperature range of test at slow cooling rate is wider than that at fast cooling rate. It can be stated that the slow cooling rate gives higher hot crack susceptibility than the fast cooling rate. In general, slow cooling rate has a wider of the solidification temperature range than the fast cooling rate for most steel grades. Solidification temperature range is proportional to the critical temperature range and it is known that the hot cracking susceptibility becomes greater as the solidification temperature range broadens [25]. Nevertheless, the growing primary dendrite at slow cooling rate is generally slower than that at fast cooling rate. Therefore it can be mentioned that the healing time of molten steel stayed between growing dendrite arms is longer than the fast one. Slow cooling rate from melting to test temperature give the specimen more time to diffuse in any direction, that means slow

cooling rate provides sufficient time for segregation of element such as sulfur during solidification. Moreover the linking up of secondary dendrite in the case of slow cooling rate is later than the other one. So the range of liquid feeding zone would be extended to lower temperature. The extending of liquid feeding zone to lower temperature directly influences the extension of ZDT downward lower temperature. So, the critical temperature range was broadened and gives more detrimental in hot crack susceptibility. For this, it seems to coincide to the reason that stated by Clyne et al. [13]. They proposed that cracks formed in the mass and liquid feeding zone are refilled with the surrounding liquid, whereas cracks formed in the cracking zone can not be refilled with the liquid because the dendrite arms are compacted enough to resist feeding of the liquid. This reason is quite agree to the reason that reported by Yamanaka et al. [8]. They pointed out that when the linked dendrite arms is slightly deformed perpendicular to the solid front, the linked arms would be ruptured. If the rupture expands to a critical amount, solute enriched molten metal will be sucked into this zone (healing). But, if the rupture is small, suction will not occur because the solid fraction of this zone is high and the permeability of molten metal is very low. They also proposed that the critical strain for internal crack formation is considered not to be the limit of

rupture, but to be the limit of the solute enriched molten metal healing. If the strain is above the critical value, the cracks will not penetrate into the shell because the rupture itself will not occur, owing to good ductility.

The critical temperature range in this study significantly depends on the strain rate when the specimen was cooled with the same cooling rate. In case of different strain rate it means different time for the tensile test. During testing at a low strain rate the materials stay a longer time at testing temperature that means a longer time provides enough time for diffusion in any direction. For tensile test at low strain rate the second dendrites have sufficient time to link up each other so that the ZST can be detected at higher temperature than that of higher strain rate. Then it results in detection of the ZDT at higher temperature. Moreover, testing at low strain rate and the solidification front advanced significantly during deformation results in the progress of the critical temperature range or the brittle zone. This reason may agree with the work of Yamanaka et al. [8]. They also concluded that at the lower strain rate the brittle zone is wider than that at high strain rate. It can be stated from their work that the critical temperature range are extending at lower

strain rates with the progress of the brittle zone, providing the effect strain exceeds the critical strain.

Nevertheless, the failure during deformation in the critical temperature range is very interesting to mention in this study. It may due to the segregation of sulfur into the interdendritic region. The sulfur segregates between solidifying dendrites and depresses the solidifying range of this steel to create liquid films in the interdendritic region. Then, even low tensile strains can cause dendritic separation and hot tears [26,27]. In this study the microstructure in the quenching test was performed to simulate the microstructure of the specimen of hot tensile test. The microstructure of the quenched specimens that correspond to the ZDT in hot tensile test of all condition has been shown in Fig.4-3 to Fig.4-6. It can be indicated that the loss of ductility may due to the precipitation of manganese sulfide. Fig.4-3 shows the microstructure, which correspond to the ZDT at 1296°C in the case of high cooling rate and low strain rate. This temperature is about 85°C apart from solidus temperature that was detected with DTA. The microstructure, which appears in Fig.4-3, seems to be the eutectic structure of sulfide. According to the work of Imagumbai [28], it can be cited that between dendrite arms of solid/liquid zone where

liquid still existed at quenching, eutectic type II manganese sulfide was predominant with iron sulfide inclusion which particularly overlapping manganese sulfide inclusion. The overlapping of iron sulfide on manganese sulfide became more frequent at location where temperature at quenching was higher than the liquidus. It is very interesting that no iron sulfide was found in the fully solidified zone before quenching the steel AISI L3 (for the condition of this study). Ito et al. [29] observed behaviors of manganese sulfide in low carbon aluminium killed steel (approx. 0.3%C-0.5%Si-0.8%Mn in mass%) under controlled solidification conditions and quenching temperatures. They reported that type II manganese sulfide inclusion grew until 1380-1350°C which, presumably, is lower than the solidus of the initial steel compositions by 100°C or more. Such manganese sulfide morphology is evidenced at lower ZDT as shown in Fig.4-4 to Fig.4-6. The figure shows that such manganese sulfide located at interdendritic boundaries, which were the last region to solidify which later become the austenite grain boundaries. It can be indicated that these sulfides are manganese sulfide that is confirmed by SEM-EDX analysis as shown in Fig.4-8. The morphology of manganese sulfide as depicted in Fig.4-10 and Fig.4-11, which represent the microstructure at the condition of low ductility in hot tensile test, also shows the same

morphology. It may be pointed out from the work of Baker [30] that these manganese sulfides are the type III manganese sulfide and they occur as perfect octahedral. These precipitates result from the concentration of strain at the grain boundaries during deformation and consequent nucleated of microvoid around the manganese sulfide precipitates. Then such microvoid will coalesce and leading to further grains boundary microvoid and fracture. However this steel contains lower Mn/S ratios about 13, so sulfur would precipitate less manganese sulfide on cooling and more available sulfur in solution. Then leading to lower ductility because of increased grain boundary segregation. Lankford [16] has indicated that in the case of low cooling rate of 0.6°C/s some manganese will be found in solution in the precipitate. As the cooling rates become slower, more manganese will have time to diffuse to the grain boundary and the precipitate will become more enriched with manganese. However if the cooling rate becomes slow enough, manganese will nucleate and manganese precipitation will dominate. Nevertheless in continuous casting process, manganese atoms are able to combine with sulfur atoms to form coarse manganese sulfide particles because of slow cooling and the very low strain rate. However if solute sulfur atoms remain during low strain rate in the continuous casting process, they will segregate to the

grain boundary precipitate/matrix interfaces as well as to the austenitic boundaries, leading to easy decohesion of the interface and consequent nucleation of microvoid.

Below complete solidification temperature the hot ductility is affected from the test variables. The variation of the reduction of area to failure with deformation temperature after cooling from melting has been shown in Fig.4-1. A different of reduction of area value at different test condition clearly be seen over the temperature range 1200-900°C. It can be indicated that the tensile test in the case slow cooling rate and slow strain rate is markedly different from other test conditions. It may due to the ZDT occur later. The reduction of area value, however, increases rapidly with decreasing temperature. In the case of slow cooling rate the reduction of area value in the case of low strain rate is higher than that in the case of high strain rate in temperature range between 1200°C and 900°C. Whilst in the case of fast cooling the reduction of area value in the case of low strain rate is higher than that in the case of high strain rate. But it occurs in temperature range between 1200°C and 1150°C. It can be clarified that low strain rate take a longer time to produce a coarser inclusion. In this case, the inclusions probably coarsen,

so that they are no longer able to pin the austenite grain boundaries. This result is similar to the work of Yasumoto et al. [19] and Thome [11]. Nevertheless, in the case of fast cooling rate the reduction of area value in the case of high strain rate is higher than that in case of low strain rate. It can be quoted from other researcher [21,22] that higher strain rate improve the hot ductility because there is insufficient time for strain induced precipitation. The amount of grain boundary sliding is reduced and there is insufficient time for the formation and diffusion controlled growth of voids around the precipitates located at the grain boundaries. It also can be found from Fig.4-1 that cooling rate also affected hot ductility, except the case of slow cooling rate and high strain rate. It is interesting to note that the reduction of area value in case of slow cooling rate is higher than that in the case of fast cooling rate. These effects can be explained in terms of the precipitation of manganese sulfide particles and their coarsening during these processes. These results agree with the report of Suzuki et al. [4]. So, it can be noted here that the improvement in hot ductility on decreasing the strain rate or cooling rate to deformation temperature from melting can also be explained similarly by the formation of manganese sulfide particles and their coarsening during these processes.

4-4 Hot ductility of steel grade AISI O1

The reduction of area and maximum load versus the test temperature of various test conditions is shown in Fig.4-13. The characteristic temperature (ZST ZDT and ΔT) of various test conditions are shown in Table 4-2.

Hot tensile test of specimen cooled at cooling rate of 0.5°C/s and slow strain rate of 2×10^{-3}/s shows ZST and ZDT to be 1415°C and 1290°C, respectively. The curve shows a distinctive maximum reduction of area above 95% in the temperature range between 1200°C and 1000°C. Then the reduction of area decline with decreasing test temperature. The curve shows the reduction of area of 70% at 900°C. Tensile test at high strain rate of 2×10^{-2}/s after slow cooling rate from melting shows ZST and ZDT to be 1405°C and 1230°C, respectively. The maximum reduction of area for this test condition appears at 1102°C with the reduction of area of 99%. The reduction of area for this test condition rapidly decline with decreasing test temperature below 1100°C and displays the reduction of area of 51% at 900°C. It can be noticed that the trend of hot ductility curve of tensile tests at high and low strain rate after being cooled from melting at slow cooling rate is the same.

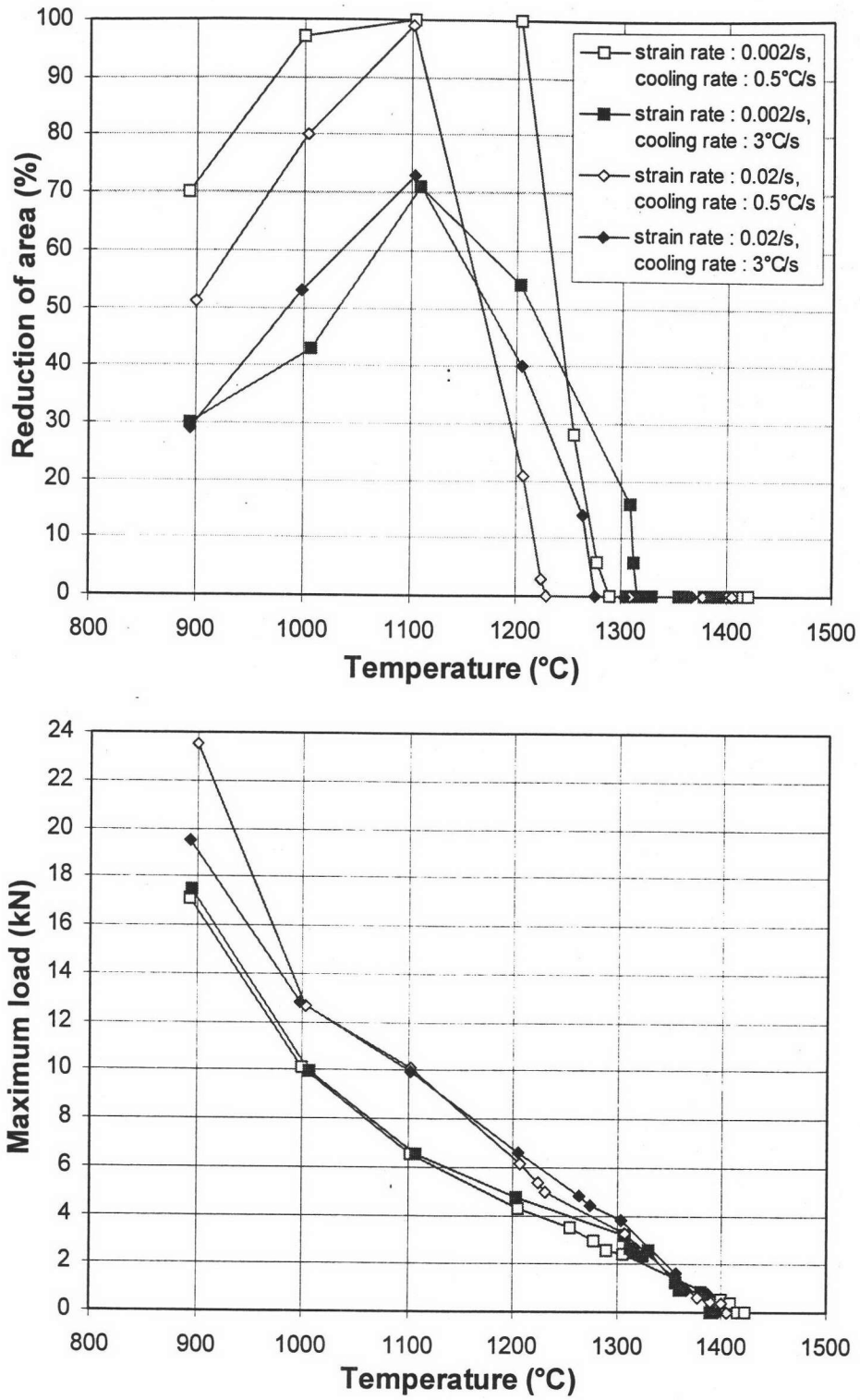

Fig.4-13 Reduction of area and the maximum tensile load versus temperature of the steel grade AISI O1.

Table 4-2 Characteristic temperatures of the steel grade AISI O1 at various test conditions

Steel grade	Test condition		ZDT	ZST	ΔT
	cooling rate (°C/s)	strain rate (/s)	(°C)	(°C)	(°C)
AISI O1	0.5	$2x10^{-3}$	1290	1415	125
	0.5	$2x10^{-2}$	1230	1405	175
	3	$2x10^{-3}$	1316	1388	72
	3	$2x10^{-2}$	1275	1395	120

For the fast cooling rate of 3°C/s, tensile test at slow strain rate of $2x10^{-3}$/s shows ZST and ZDT to be 1388°C and 1316°C, respectively. The curve displays the maximum reduction of area of 71% at 1108°C. Then the reduction of area decreased with decreasing test temperature and shows the reduction of area of 30% at 895°C. The ZST and ZDT for the test at high strain rate of $2x10^{-2}$/s are 1395°C and 1275°C, respectively. The curve for this test condition reveals the maximum reduction of area of 73% at 1103°C and then decline to 29% at 894°C. It can be documented that the ZDT for both slow and fast cooling rate is decreased with increasing strain rate. The critical temperature range ΔT for both low and fast cooling rate is widened with increasing strain rate.

Moreover, Table 4-2 indicated that the fast cooling rate from melting resulted in shifting the ZDT toward higher temperature. The critical temperature range of fast cooling rate is smaller than slow cooling rate. Fig.4-14 shows the summary of effect of cooling rate on critical temperature at various strain rates. It can be noticed that under the condition of this study the critical temperature range is narrowed with increasing cooling rate for both tests at high and low strain rate. Tensile test at slow strain rate has effect in reducing the critical temperature range for both high and low cooling rates.

4.5 Metallographical investigation of steel grade AISI O1

The microstructure shown in Fig.4-15 represents the structure in the specimen that quenched from 1316°C after cooled from melting with cooling rate of 3°C/s. This figure shows the eutectic structure and small white area located along interdendritic boundaries. Fig.4-16 shows the microstructure of the specimen that quenched from 1275°C with the same cooling rate shown in Fig-15. Fig.4-17 and Fig.4-18 show the microstructure of the microstructure of the specimen which quenched from 1290°C

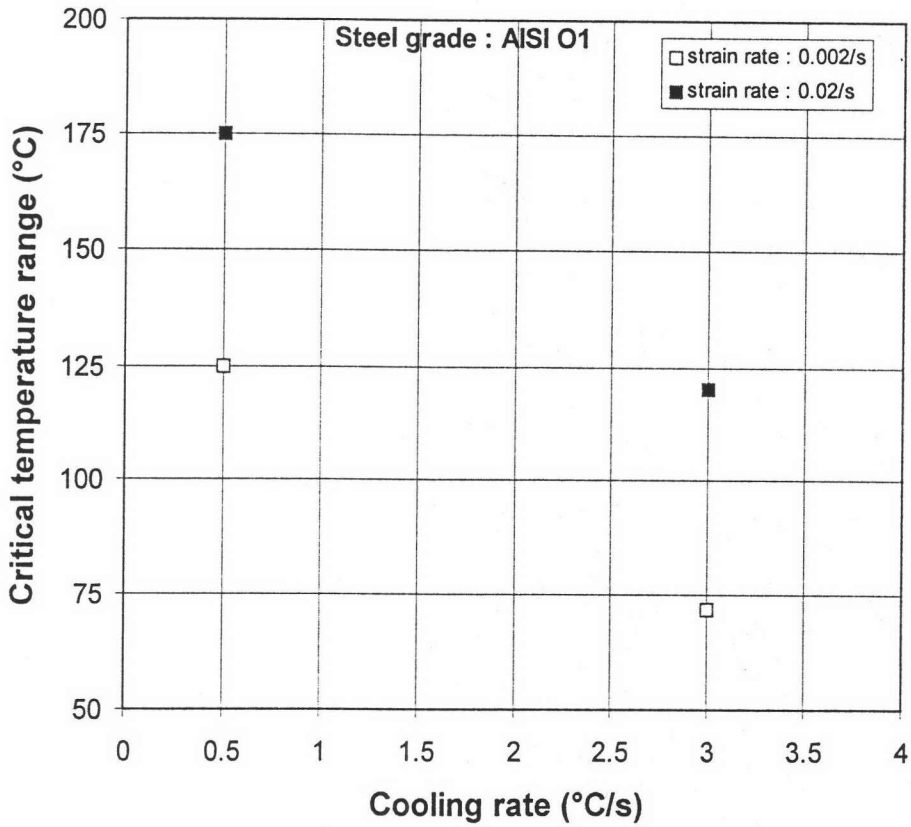

Fig.4-14 Characteristic temperature range between ZDT and ZST of steel grade AISI O1.

and 1230°C after solidified from melting at cooling rate of 0.5°C /s, respectively. Fig.4-16 to Fig.4-18 are also show the eutectic structure and the white area along interdendritic boundaries. The white area is believed to be liquid phase and remains along the interdendritic boundaries at ZDT which, later, become the austenite grain boundaries. The eutectic structure is identified with SEM-EDX. The SEM-micrograph shown in Fig.4-19

represents the structure as those appear in Fig.4-15 to Fig.4-18. The identified spectrum of the eutectic structure is shown in Fig.4-20 while Fig.4-21 shows the identified spectrum of the matrix. The elements were identified with SEM-EDX shown in Fig.4-20 as W, V, Cr and Fe. Whilst the matrix identified with SEM-EDX were Fe. Fig.4-22 shows microstructure of the specimen, which is quenched from 900°C after cooled from melting at cooling rate of 3°C/s. This temperature correspond to the temperature in hot tensile test as the reduction of area indicated to be about 30% for both high and low strain rate. Fig.4-23 shows the SEM-micrograph of the same sample shown in Fig.4-22. The precipitate that appears in the figure is then identified with SEM-EDX and shows its spectrum in Fig.4-24. The identified spectrum indicated that the precipitates are the element of W, V, Cr and Fe.

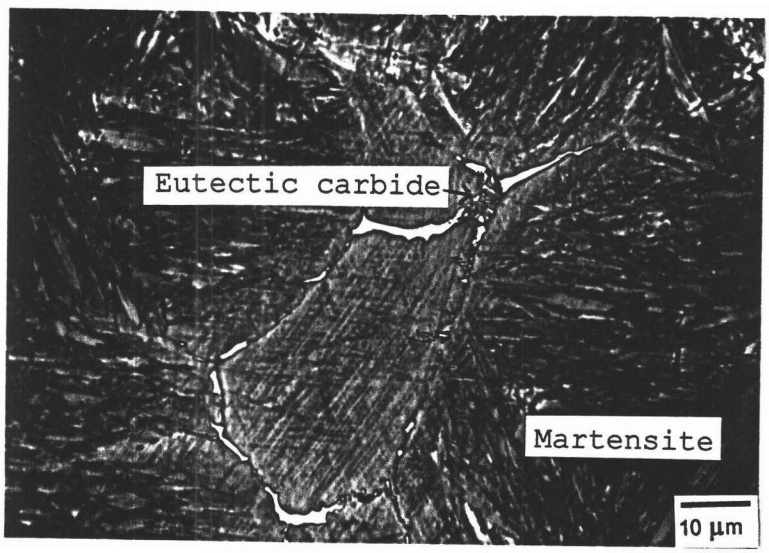

Fig.4-15 Carbides precipitates along austenite grain boundaries of specimen that solidified from melting with cooling rate of 3°C/s to 1316°C and then quenched.

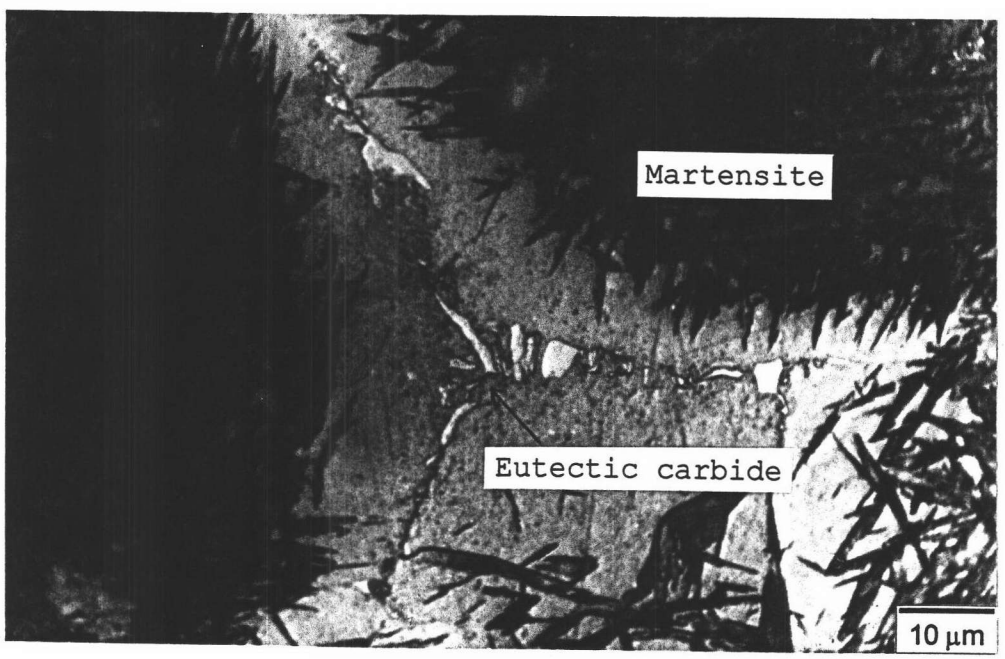

Fig.4-16 Carbides precipitates along austenite grain boundaries of specimen that solidified from melting with cooling rate of 3°C/s to 1275°C and then quenched.

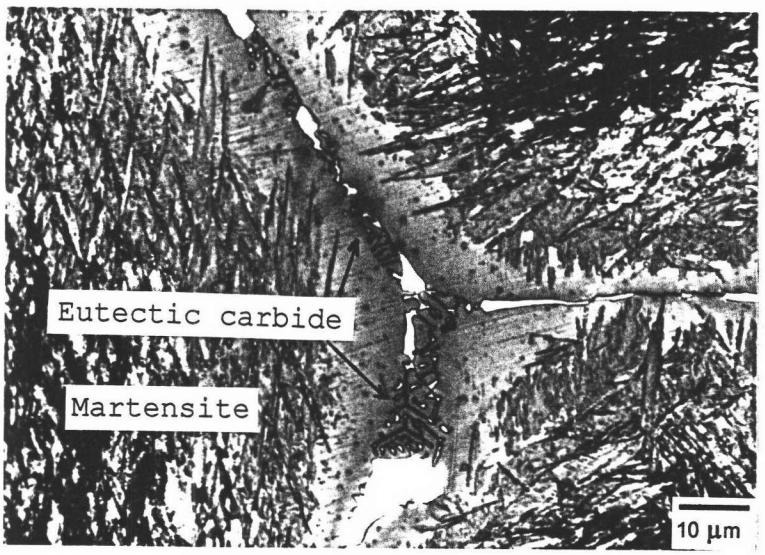

Fig.4-17 Carbides precipitates along austenite grain boundaries of specimen that solidified from melting with cooling rate of 0.5°C/s to 1290°C and then quenched.

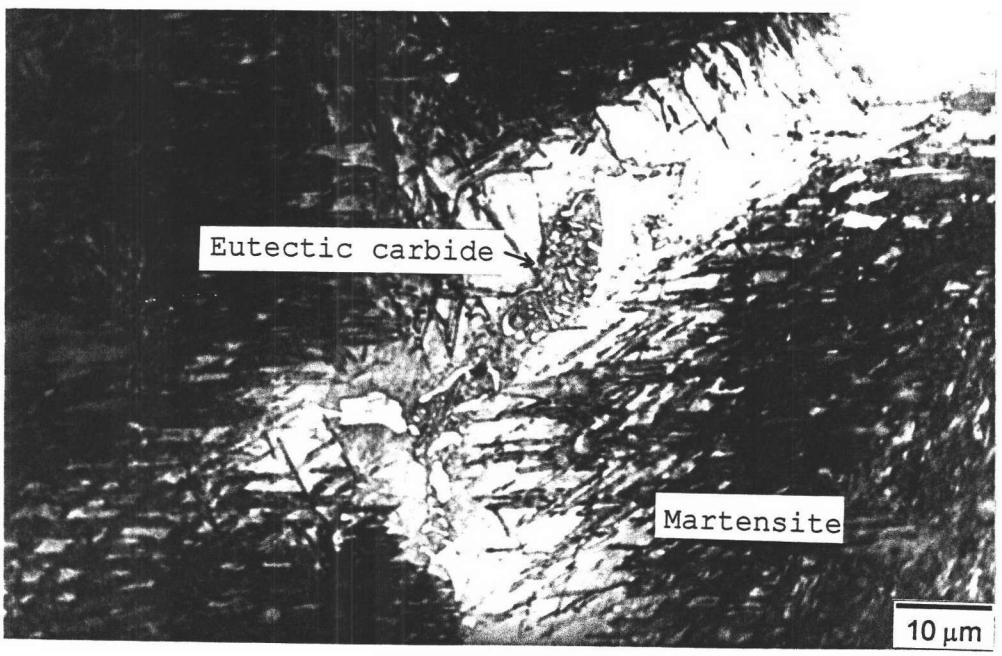

Fig.4-18 Carbides precipitates along austenite grain boundaries of specimen that solidified from melting with cooling rate of 0.5°C/s to 1230°C and then quenched.

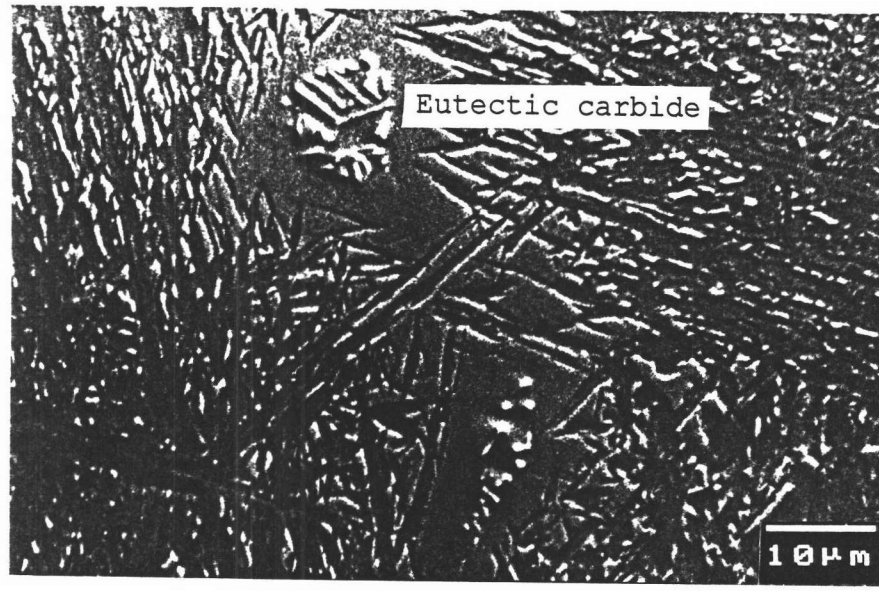

Fig.4-19 SEM-micrograph of carbide precipitates of specimen that solidified from melting with cooling rate of 3°C/s to 1292°C and then quenched.

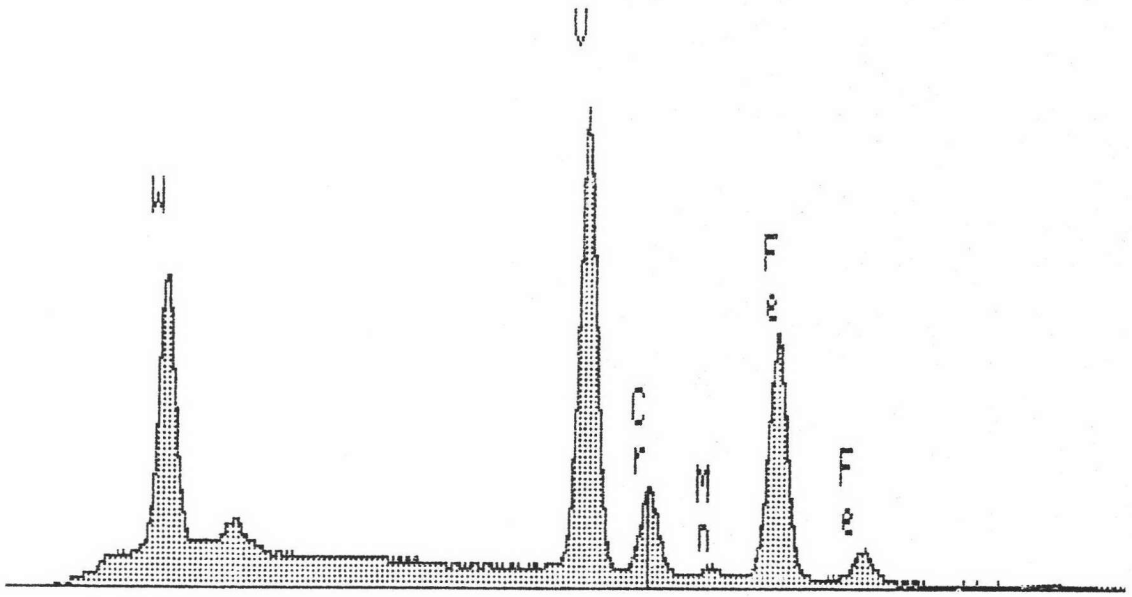

Fig.4-20 SEM-EDS analysis of carbide precipitates of W, V Cr and Fe of specimen that solidified from melting with cooling rate of 0.5°C/s to 1292°C and then quenched.

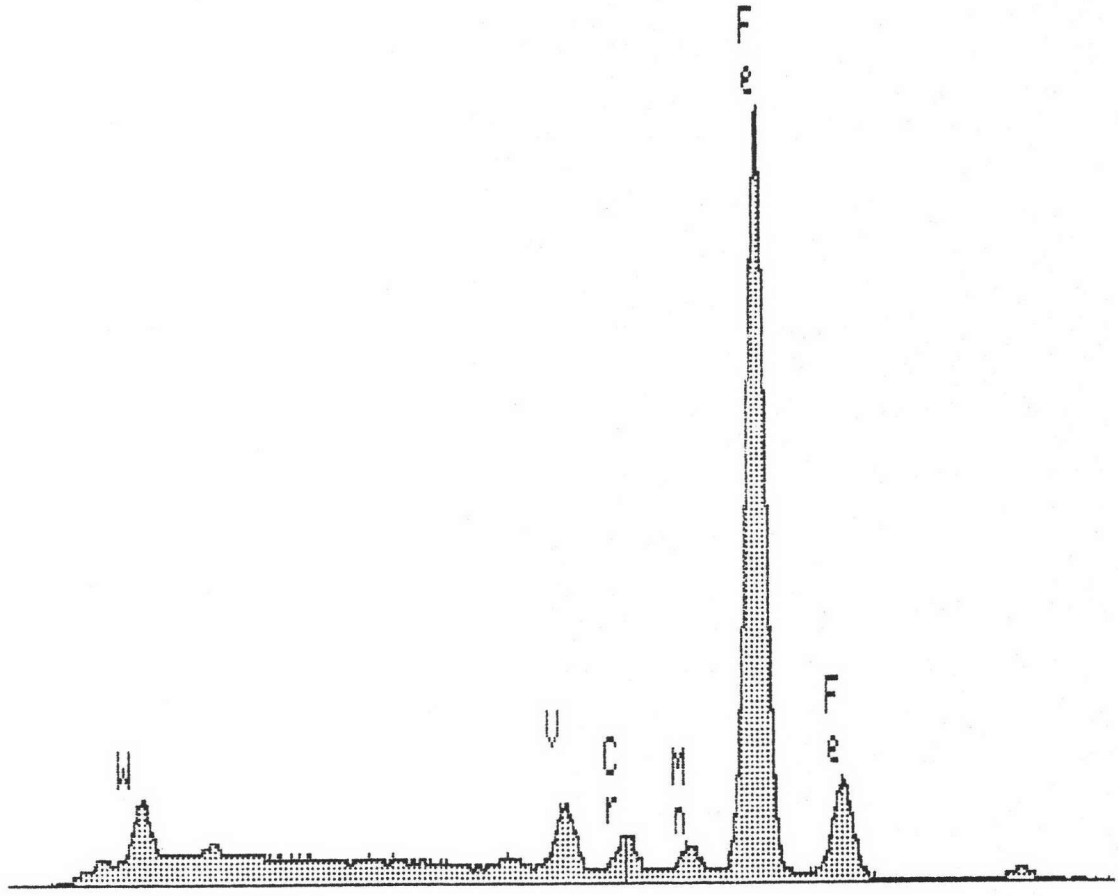

Fig.4-21 SEM-EDS analysis of the matrix of specimen that solidified from melting with cooling rate of 0.5°C/s to 1292°C and then quenched.

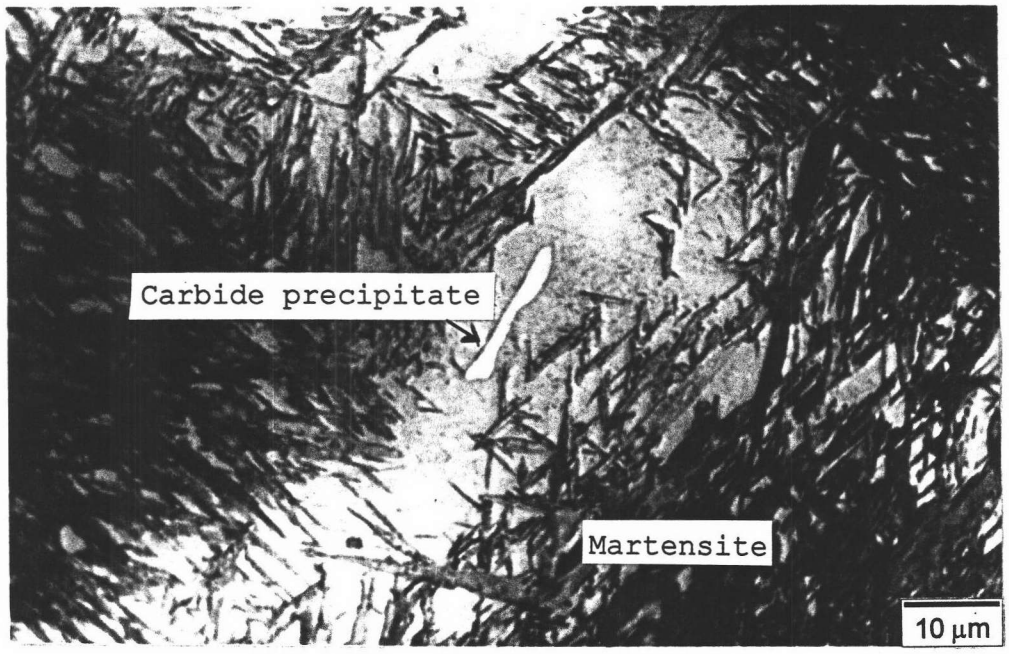

Fig.4-22 Carbides precipitates along austenite grain boundaries of specimen that solidified from melting with cooling rate of 3°C/s to 900°C and then quenched.

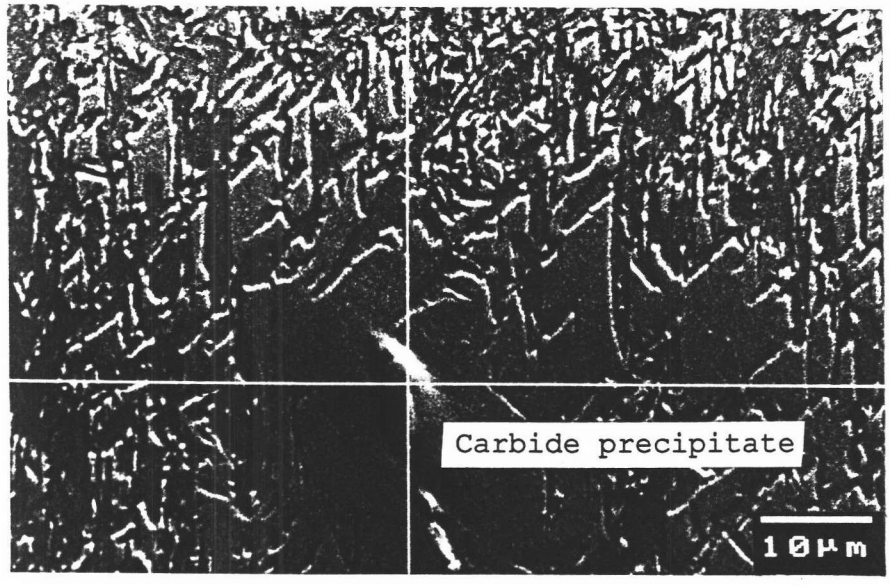

Fig.4-23 SEM-micrograph of carbide precipitate of specimen that solidified from melting with cooling rate of 3°C/s to 900°C and then quenched.

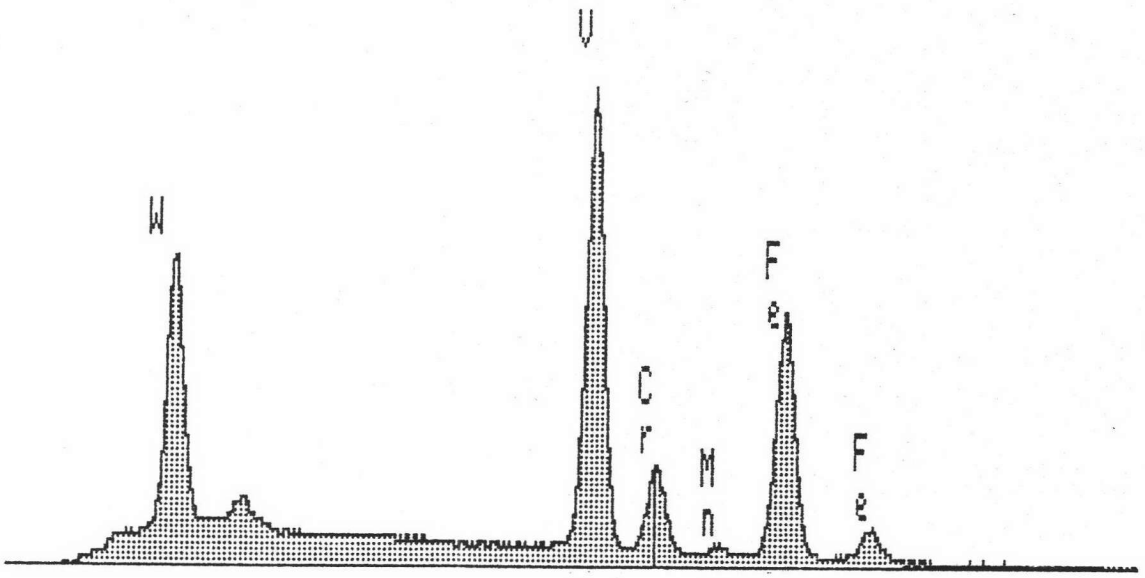

Fig.4-24 SEM-EDS analysis of carbide precipitates of W, V Cr and Fe of specimen that solidified from melting with cooling rate of 3°C/s to 900°C and then quenched.

4.6 Effect of cooling rate and strain rate on hot ductility of steel grade AISI O1

The result of hot tensile test is shown in Fig.4-13 and Table 4-2. It can be demonstrated from the results that the tensile test at various strain rates of the specimen cooled from melting at cooling rate affected the widening of critical temperature range.

Trend of the critical temperature range for this steel is similar to steel grade AISI L3. This is interesting to be documented here again that the slow cooling rate results in higher hot crack susceptibility than that of fast cooling rate. Because the critical temperature range in the former condition is wider than the latter condition. The mechanisms of extending the critical temperature due to the effect of test variable should be the same mechanism as that proposed in section 4-3. The critical temperature range is shown for comparing between steel grade AISI O1 and AISI O3. The critical temperature range of this steel is shifted to higher temperature when compared to steel grades AISI L3. Therefore the temperature range of hot crack susceptibility is higher than that of steel grade AISI L3. However the carbide forming elements of this steel grade is relatively high in comparing to steel grade AISI L3.

Steel grade AISI O1 contains the special carbide forming elements V, Mo and W. The hot crack susceptibility may be caused by such carbide precipitation occurred in the solidified structure.

The microstructures of quenched specimen at ZDT that correspond to the ZDT in hot tensile test of all test conditions are shown in Fig.4-15 to Fig.4-18. These figures show that residual melt is remaining in the structure. These figure also reveal the eutectic carbide structure located along grain boundaries. SED-EDX analysis of these eutectic structures is shown in Fig.4-20 whereas the spectrum of the matrix is shown in Fig.4-21. From the analysis this eutectic carbide is, presumably, the carbide of W, V and Cr. The microstructure in the condition of low reduction of area value at 900°C was shown in Fig.4-22 and its spectrum was shown in Fig.4-24. From the analysis it is interesting to indicate that this precipitate may be the carbide of W and V. The occurrence of this carbide in the structure may cause hot cracking when it is subjected to deformation. If tensile stresses occur, the specimen shows brittle fracture as long as remaining melt exist or the softening of the materials is restrained by large amounts of these carbide precipitates.

It is also interesting to note that the hot ductility of steel grade AISI O1 in the temperature ranges between 1000°C and 900°C is strongly depend on the strain rate and cooling rate. But the hot tensile tests in the condition of high cooling rate no different in reduction of area value. An increasing in strain rate in the case of low cooling rate leads to a drastic decline in reduction of area value for this steel. However this steel grade behaves in a similar way to the steel grade AISI L3 regarding their hot ductility behaviors in depending on the cooling rate and strain rate.